

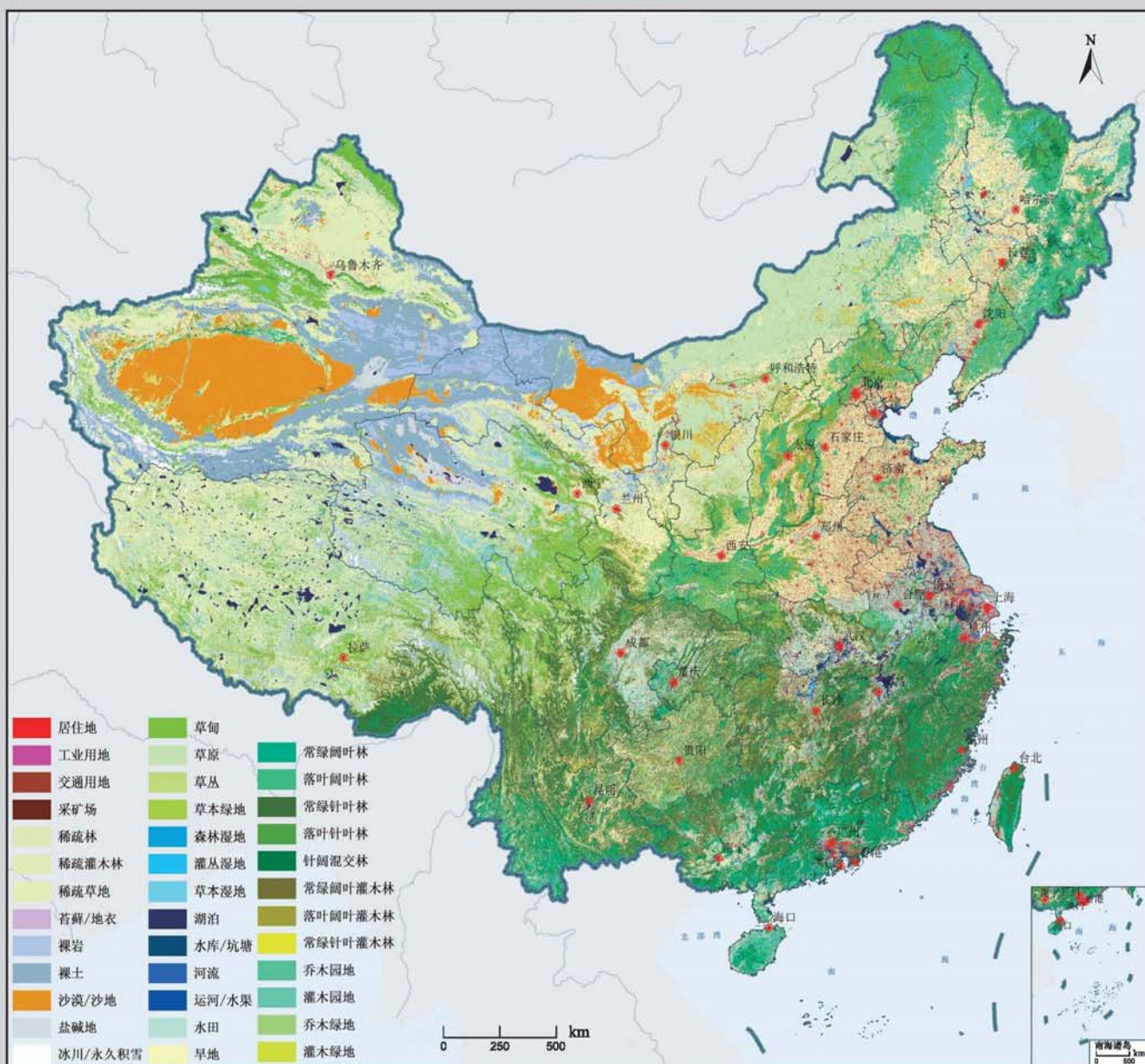
科学出版社
出版
中国地理学会环境遥感分会
中国科学院遥感与数字地球研究所
主办

JOURNAL OF REMOTE SENSING

遥感学报

2013年 Vol.17 第17卷 No.4 第4期 ISSN 1007-4619 CN11-3841 / TP CODEN YXAUAB

2010年中国土地覆被遥感监测数据集 (ChinaCover2010)



综述

森林垂直结构参数遥感反演综述 赵静, 李静, 柳钦火 (707)

基础理论

HASM 解算的 2 维双连续投影方法 闫长青, 岳天祥, 赵刚, 王晨亮 (722)

地形起伏度最佳分析区域预测模型 张锦明, 游雄 (735)

技术方法

运用 GVF Snake 算法提取水域的不规则边界 朱述龙, 孟伟灿, 朱宝山 (750)

全景立体视觉的快速近区重力地形改正方法 邸凯昌, 吴凯, 刘召芹, 万文辉, 邸志众, 李钢 (767)

利用氧气和水汽吸收波段暗像元假设的 MERIS 影像二类水体大气校正方法
檀静, 李云梅, 赵运林, 吕恒, 徐德强, 周莉, 刘阁 (778)

自然语言理解的中文地址匹配算法 宋子辉 (795)

3 维地形的金字塔上下采样局部实时简化算法 易雄鹰, 方超 (809)

面向对象分类特征优化选取方法及其应用 王贺, 陈劲松, 余晓敏 (822)

针对 Terra/MODIS 数据的改进分裂窗地表温度反演算法
RI Changin, 柳钦火, 历华, 方莉, YU Yunyue, SUN Donglian (840)

基于 Voronoi 几何划分和 EM/MPM 算法的多视 SAR 图像分割 赵泉华, 李玉, 何晓军, 宋伟东 (847)

遥感应用

地面成像光谱数据的田间杂草识别 李颖, 张立福, 严薇, 黄长平, 童庆禧 (863)

耦合遥感观测和元胞自动机的城市扩张模拟 张亦汉, 黎夏, 刘小平, 乔纪纲, 何执兼 (879)

结合凝聚层次聚类的极化 SAR 海冰分割 于波, 孟俊敏, 张晰, 纪永刚 (896)

杭州湾 HJ CCD 影像悬浮泥沙遥感定量反演 刘王兵, 于之锋, 周斌, 蒋锦刚, 潘玉良, 凌在盈 (912)

“灰霾遥感”专栏

北京区域 2013 严重灰霾污染的主被动遥感监测
李正强, 许华, 张莹, 张玉环, 陈澄, 李东辉, 李莉, 侯伟真, 吕阳, 顾行发 (924)

利用细模态气溶胶光学厚度估计 $PM_{2.5}$ 张莹, 李正强 (936)

利用太阳-天空辐射计遥感观测反演北京冬季灰霾气溶胶成分含量
王玲, 李正强, 马奕, 李莉, 魏鹏 (951)

利用 HJ-1 CCD 高分辨率传感器反演灰霾气溶胶光学厚度 张玉环, 李正强, 侯伟真, 许华 (964)

基于地基遥感的灰霾气溶胶光学及微物理特性观测
谢一淞, 李东辉, 李凯涛, 张龙, 陈澄, 许华, 李正强 (975)

利用激光雷达探测灰霾天气大气边界层高度 张婉春, 张莹, 吕阳, 李凯涛, 李正强 (987)

北京区域冬季灰霾过程中人为气溶胶光学厚度估算 王堰, 谢一淞, 李正强, 李东辉, 李凯涛 (1000)

结合地基激光雷达和太阳辐射计的气溶胶垂直分布观测
吕阳, 李正强, 尹鹏飞, 许华, 李凯涛, 张婉春, 侯伟真 (1014)

灰霾污染状况下气溶胶组分及辐射效应的遥感估算
魏鹏, 李正强, 王堰, 谢一淞, 张莹, 许华 (1026)

JOURNAL OF REMOTE SENSING

(Vol. 17 No. 4 July, 2013)

CONTENTS

Review

Review of forest vertical structure parameter inversion based on remote sensing technology
..... ZHAO Jing, LI Jing, LIU Qinhua (697)

Fundamental Research

Two-dimensional double successive projection method for high accuracy surface modeling
..... YAN Changqing, YUE Tianxiang, ZHAO Gang, WANG Chenliang (717)

A prediction model of optimum statistical unit of relief ZHANG Jinming, YOU Xiong (728)

Technology and Methodology

Irregular water boundary extraction using GVF snake ZHU Shulong, MENG Weican, ZHU Baoshan (742)

Fast near-region gravity terrain correction approach based on panoramic stereo vision
..... DI Kaichang, WU Kai, LIU Zhaoqin, WAN Wenhui, DI Zhizhong, LI Gang (759)

Atmospheric correction of MERIS data on the black pixel assumption in oxygen and water vapor absorption
bands TAN Jing, LI Yunmei, Zhao Yunlin, LV Heng, XU Deqiang, ZHOU Li, LIU Ge (768)

Address matching algorithm based on chinese natural language understanding SONG Zihui (788)

Local real-time simplification algorithm for three-dimensional terrain using up and down sampling and
pyramid theory YI Xiongying, FANG Chao (802)

Feature selection and its application in object-oriented classification
..... WANG He, CHEN Jinsong, YU Xiaomin (816)

Improved split window algorithm to retrieve LST from Terra/MODIS data
..... RI Changin, LIU Qinhua, LI Hua, FANG Li, YU Yunyue, SUN Donglian (830)

Multi-look SAR image segmentation based on voronoi tessellation technique and EM/MPM algorithm
..... ZHAO Quanhua, LI Yu, HE Xiaojun, SONG Weidong (841)

Remote Sensing Applications

Weed identification using imaging spectrometer data
..... LI Ying, ZHANG Lifu, YAN Wei, HUANG Changping, TONG Qingxi (855)

Urban expansion simulation by coupling remote sensing observations and cellular automata
..... ZHANG Yihan, LI Xia, LIU Xiaoping, QIAO Jigang, HE Zhijian (872)

Segmentation method for agglomerative hierarchical-based sea ice types using polarimetric SAR data
..... YU Bo, MENG Junmin, ZHANG Xi, JI Yonggang (887)

Assessment of suspended sediment concentration at the Hangzhou Bay using HJ CCD imagery
..... LIU Wangbing, YU Zhifeng, ZHOU Bin, JIANG Jingang, PAN Yuliang, LING Zaiying (905)

(to be continued to Inside Back Cover)

(continued from Contents page)

Haze: Remote Sensing

- Joint use of active and passive remote sensing for monitoring of severe haze pollution in Beijing 2013
..... *LI Zhengqiang, XU Hua, ZHANG Ying, ZHANG Yuhuan, CHEN Cheng, LI Donghui, LI Li,*
..... *HOU Weizhen, LV Yang, GU Xingfa* (919)
- Estimation of PM_{2.5} from fine-mode aerosol optical depth *ZHANG Ying, LI Zhengqiang* (929)
- Retrieval of aerosol chemical composition from ground-based remote sensing data of sun-sky radiometers
during haze days in Beijing winter *WANG Ling, LI Zhengqiang, MA Yan, LI Li, WEI Peng* (944)
- Retrieval of haze aerosol optical depth based on high spatial resolution CCD of HJ-1
..... *ZHANG Yuhuan, LI Zhengqiang, HOU Weizhen, XU hua* (959)
- Aerosol optical and microphysical properties in haze days based on ground-based remote sensing measurements
..... *XIE Yisong, LI Donghui, LI Kaitao, ZHANG Long, CHEN Cheng, XU Hua, LI Zhengqiang* (970)
- Observation of atmospheric boundary layer height by ground-based LiDAR during haze days
..... *ZHANG Wanchun, ZHANG Ying, LV Yang, LI Kaitao, LI Zhengqiang* (981)
- Anthropogenic aerosol optical depth during days of high haze levels in the Beijing winter
..... *WANG Yan, XIE Yisong, LI Zhengqiang, LI Donghui, LI Kaitao* (993)
- Joint use of ground-based LiDAR and sun-sky radiometer for observation of aerosol vertical distribution ...
..... *LV Yang, LI Zhengqiang, YIN Pengfei, XU Hua, LI Kaitao, ZHANG Wanchun, HOU Weizhen* (1008)
- Remote sensing estimation of aerosol composition and radiative effects in haze days
..... *WEI Peng, LI Zhengqiang, WANG Yan, XIE Yisong, ZHANG Ying, XU Hua* (1021)

Fast near-region gravity terrain correction approach based on panoramic stereo vision

DI Kaichang¹, WU Kai¹, LIU Zhaoqin¹, WAN Wenhui¹, DI Zhizhong², LI Gang²

1. State Key Laboratory of Remote Sensing Science, Jointly Sponsored by the Institute of Remote Sensing and Digital Earth, Chinese Academy of Sciences and Beijing Normal University, Beijing 100101, China;
2. Beijing Explo-Tech Engineering Co., Ltd., Beijing 100085, China

Abstract: Gravity terrain correction is a critical step in regional gravity survey. The main challenge for gravity terrain correction is how to rapidly and inexpensively reconstruct high-quality terrain near the gravity survey station. This paper proposes a fast near-region terrain correction approach based on panoramic stereo vision and photogrammetry techniques. A fast and low-cost topographic mapping system is designed and developed for this purpose. To miniaturize the system and assure required mapping accuracy, we theoretically analyze and optimize the hardware design. The developed software system generates DEM automatically from panoramic stereo images and calculates the gravity correction value at each station. The system has been verified in several filed tests with various terrain circumstances. The test results demonstrate that the developed gravity terrain correction method significantly outperforms the traditional field surveying methods in efficiency and accuracy.

Key words: gravity terrain correction, topographic mapping, panoramic vision, stereo image matching, point cloud filtering

CLC number: TP79 **Document code:** A

Citation format: Di K C, Wu K, Liu Z Q, Wan W H, Di Z Z and Li G. 2013. Fast near-region gravity terrain correction approach based on panoramic stereo vision. *Journal of Remote Sensing*, 17(4): 759–767 [DOI: 10.11834/jrs.20132218]

1 INTRODUCTION

Gravity terrain correction is an important procedure for obtaining Bouguer gravity anomaly during regional gravity survey (Yen, et al., 1994). Terrain correction is normally categorized into three parts by the range from the gravity station, one part being correction for terrain relatively close to the survey station as far as 20—50 m, commonly known as near region terrain correction (Fan, 2007), while the other two parts for more distant terrain, referred as mid region terrain correction and far region terrain correction. Currently, for the mid and far region parts, computer aided programs have been introduced to automate the terrain correction procedure based on widely available topographic databases (Cogbill, 1990). However, this is often not the case for near region part when large-scale topographic product doesn't exist, especially in mountainous areas (Jia, et al., 2009). As gravitational effects become decreased in proportional to the distance from the survey station, near-region terrain correction is more critical than mid and far region correction.

A systematic methodology for performing terrain correction was developed by Hammer (1939). In his method, a template consisting of a series of circles is applied and the center of the

circles is placed over the gravity station on the map. Amounts of prisms with increased distance from the center are subsequently made to estimate their individual gravity effect with a formula. By accumulating all the prism's effects, terrain correction is finished for the gravity station. The practical manual manipulation of Hammer's method is not only complex but also fails to guarantee an accurate value concerning the variation of terrain. Though an improvement was made later by adapting Hammer's formula to be easily implemented by computer (Bott, 1959; Kane, 1962; Nagy, 1966), the accuracy problem still remains to be resolved, especially in mountainous areas. Further research has concluded that the Hammer's method could be refined by using smaller patches or by defining the surface shape more precisely (Campbell, 1980; Zhou, et al., 1990; Parker, 1996). According to China's large-scale gravity exploration specification, the Root Mean Square Error (RMSE) of near region terrain correction (0—20 m) should be within 0.025 mgal ($1 \text{ mgal} = 10^{-3} \text{ cm/s}^2$) (Sun & Ding, 1997). For such a high precision gravity survey, the near region terrain correction requires a large scale topographic map (1:2000) or DEM with height accuracy of better than 1 m. As such a large scale topographic product often does not exist in mountainous areas, in

Received: 2012-07-17; **Accepted:** 2012-12-26; **Version of record first published:** 2013-01-03

Foundation: National Basic Research Program of China (973 program) (No.2012CB719902); National Natural Science Foundation of China (No.41171355); Funding by Beijing Explo-Tech Engineering Co., Ltd.

First author biography: DI Kaichang (1967—), male, professor. His current research interests are planetary mapping and remote sensing, rover navigation and localization. E-mail: kcidi@irsa.ac.cn

practice near region gravity survey usually involves a great deal of manual work. The surveyor usually has to make a large number of measurements using surveying instruments (e.g., a leveling instrument, theodolite or total station) in order to reconstruct the topography (Klinge, 1980). Although high precision topographic correction would be expected in this way, this classical method is time-consuming and costly, which makes it impossible to be widely used in gravity survey work when dealing with a very rugged topography. In fact, in practical procedure, near region gravity survey has long been neglected or simplified in consideration of efficiency and economic reasons, which deteriorates the accuracy of gravity survey to some extent (Leanman, 1998). Some studies (Yen, et al., 1994; Yang, et al., 2011) have shown that the amount of terrain correction is closely related to near region topography and near region correction can never be ignored in mountainous areas with high relief. Generally, topographic relief plays such an important role that most correction value in these areas is over 20 mgal or even larger, while in flat areas, the smaller correction value can almost be ignored (Li, et al., 2011). It is highly desirable to develop simple, efficient and high precision near region terrain correction method for mountainous areas.

As large part in middle and western China are mountainous areas, near region correction must be carefully and efficiently performed in such large areas. It's apparent that the main challenge for gravity terrain correction is how to rapidly and inexpensively reconstruct high-quality terrain relatively close to the gravity survey station, e.g., within a range of 30 m (Di, et al., 2011). In traditional field surveying, the surveyor divides the near region zone into 8 quadrants centering at the gravity station and makes measurements of a number of points (e.g., five points) evenly in each quadrant using total station. Generally, it takes about 20 minutes to measure nearly 40 points for each station and even more time for office work of post processing. In this research, we develop a fast near region terrain correction approach that significantly outperforms the traditional approach. It can automatically generate about 6000 three-dimensional points within two minutes (including data acquisition and data processing). This new approach is based on panoramic stereo vision and photogrammetry techniques. As the attainable accuracy of this method is largely determined by the measurement accuracy, a theoretical analysis of the measurement accuracy at different distances is performed and a suitable set of geometric configurations of stereo vision is chosen. Accordingly, a fast and low-cost topographic mapping system is designed and developed, including hardware and software for data acquisition and processing. In the field tests with various terrain circumstances, our method has proved its efficiency, accuracy and robustness compared to traditional field surveying approach.

It is worth to note that panoramic imaging technology has been widely used in "street view" image acquisition for web mapping services, such as Google Earth; stereo panoramic images have been used in navigation and mapping on the Mars exploration rover mission (Di & Li, 2007; Di & Ge, 2011). The contribution of this paper is to introduce the stereo panoramic vision technology into the field of gravity terrain correction and to design and develop a fast and low-cost topographic mapping

system for practical application in near-region gravity terrain correction.

2 HARDWARE DESIGN AND THEORETICAL ACCURACY ANALYSIS

2.1 Hardware design of the topographic mapping system

The measurement accuracy of a stereo mapping system is largely determined by its hardware design. As is shown in Fig.1, the hardware of the system includes a pair of CCD cameras for stereo image acquisition, a rotary stage to rotate the cameras, and a tripod for holding the imaging system. The stereo cameras are mounted on the two ends of a camera bar, which is fixed to the two-degree-of-freedom rotary stage. The rotary stage can rotate $\pm 180^\circ$ horizontally and $\pm 36^\circ$ vertically so that the system acquires panoramic stereo images around a gravity station. A laptop computer is used to control the cameras and the rotary stage.



Fig.1 Hardware of the topographic correction system

The geometric configuration parameters of the hardware components are listed in Table 1.

Table 1 Geometric parameters of the stereo camera system

Stereo camera	Camera type	MV-VE141SC/SM
	Stereo base	50 cm
	Focal length	12 mm
	Image dimension	1392×1040 pixels
	Pixel size	6.45 μm ×6.45 μm
Rotary stage	Vertical range	-36° — 36°
	Horizontal range	-180° — 180°
	Accuracy	0.0129°
Laptop computer	CPU	Intel core i3 , 2.13 GHz

These hardware components are determined by the following theoretical analysis of measurement accuracy. The idea is to select the low-cost but reliable components that satisfy the accuracy requirement of near-region gravity terrain correction, rather than to select high-end components that achieve the highest accuracy.

2.2 Theoretical analysis of measurement accuracy

In order to perform near region terrain correction, it is

important to analyze the attainable measurement accuracy of the stereo camera system. Actually, the selection of camera and the setting of the baseline (Table 1) are based on theoretical measurement accuracy analysis. In our hardware system, the principal rays of the two cameras are parallel to each other and perpendicular to the baseline as depicted in Fig.2.

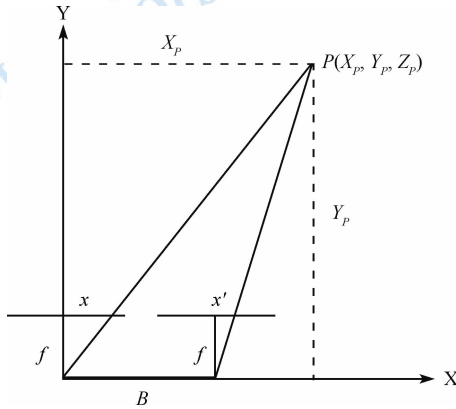


Fig.2 “Normal case” stereo configuration (Di & Li, 2007)

For such a “normal case” stereo configuration, the three dimensional coordinates of object point $P(X_p, Y_p, Z_p)$ can be calculated using the following parallax equations,

$$\begin{cases} Y_p = \frac{B}{p}f \\ X_p = \frac{B}{p}x = \frac{Y_p}{f}x \\ Z_p = \frac{B}{p}y = \frac{Y_p}{f}y \end{cases} \quad (1)$$

where f is the focal length of the camera, B is the length of stereo baseline, p is the stereo parallax of the corresponding points, which is calculated as $p = x - x'$, here taking x and x' to be the horizontal position of the points in the left and right image, respectively (Fig.2).

Based on Eq.(1), the attainable accuracy is obtained from theoretical derivation. Through error propagation, the accuracies (standard errors $\sigma_Y, \sigma_X, \sigma_Z$) are represented as (Di & Li, 2007; Di & Peng, 2011)

$$\begin{cases} \sigma_Y = \frac{Y_p^2}{Bf} \sigma_p \\ \sigma_X = \sqrt{\left(\frac{Y_p^2}{Bf}\right)^2 \left(\frac{x}{f}\right)^2 \sigma_p^2 + \left(\frac{Y_p}{f}\right)^2 \sigma_x^2} \\ \sigma_Z = \sqrt{\left(\frac{Y_p^2}{Bf}\right)^2 \left(\frac{y}{f}\right)^2 \sigma_p^2 + \left(\frac{Y_p}{f}\right)^2 \sigma_y^2} \end{cases} \quad (2)$$

where σ_p is the parallax measurement error, σ_x and σ_y are the image measurement errors in X and Y directions in image space. From Eq.(2), we can easily come to a qualitative conclusion that the measurement error reduces when the focal length and the baseline length increase. This suggests that larger focal length and baseline are preferable if possible. It is obvious that the range error σ_Y is proportional to the square of the range Y_p and that the measurement errors in X and Z directions are dependent on not only the range, but also the position of the object in the image. At a given range, the minimum error of X direction lies on the vertical line passing through the image

center (where $x = 0$), while the maximum errors of X direction lie on the left and right margins of the image. Similarly, at a given range, the minimum error of Z lies on the horizontal line passing through the image center (where $y = 0$), while the maximum errors of Z direction lie on the top and bottom margins of the image.

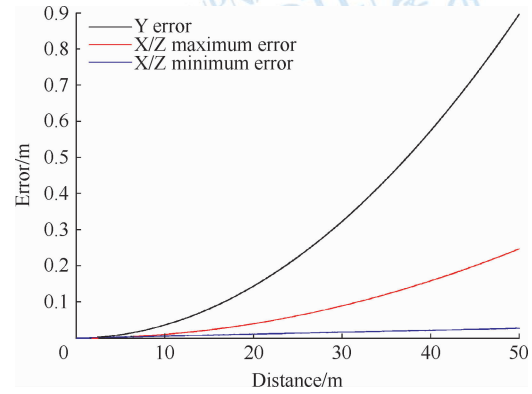


Fig.3 Theoretical measurement accuracy at different ranges

The parallax measurement accuracy is determined by the accuracy of image matching. According to a theoretical analysis, pixel-level image matching (correlation) has an accuracy of about 1/3 pixel (Zhang & Zhang, 1997), while least-squares matching has an even higher accuracy. Given $\sigma_p = 1/3$ pixel, $\sigma_x = \sigma_y = 1$ pixel, and the parameters of the cameras, the standard errors at different ranges are calculated by Eq. (2) and shown in Fig.3.

As is clearly seen in Fig.3, the measurement error in the range direction is always larger than that in the other two directions, and measurement accuracies in three directions are all better than 1 m within 50 m, which satisfies the requirements of near region terrain correction.

2.3 Calibration of stereo cameras

It is critical to calibrate the cameras in order to achieve the theoretical mapping accuracy. The task of camera calibration is to determine the interior orientation parameters (focal length, position of principal point) and optical distortion parameters of each camera, and the relative orientation parameters between the two cameras.

Camera calibration is performed at a calibration range where hundreds of precisely measured control points are evenly distributed in a three dimensional space (Fig.4). The internal camera model used in this calibration is very similar to that used by Heikkila and Silven (1997), which can generally deal with camera distortion very efficiently. To reduce the time of manual measurement of the control points in the images, we developed a semi-automatic method for control point measurement. We only need to manually measure several control points (green crosses in Fig.4), then the rest of control points (red crosses in Fig.4) are extracted automatically by least squares template matching. As we can see, most control points in the image are extracted successfully, which are sufficient for camera calibration. Based on these control points, interior orientation parameters, optical distortion parameters, and exterior orientation parameters are determined

through a least squares solution of space resection with collinearity equations (Feng, 2002). The accuracy of camera calibration is evaluated by the root mean square residual on the control points, which turned out to be within 0.2 pixel for both the left and right camera.

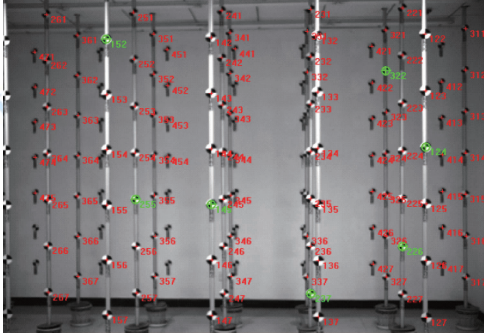


Fig.4 Camera calibration range

In order to calibrate the relative orientation and translation of the two cameras, images of the three dimensional calibration range are captured simultaneously by the stereo cameras. Multiple pairs of images are used to improve accuracy and robustness in the calibration. After calibration, we get the left camera's position vector T_{left} and orientation matrix R_{left} , right camera's position vector T_{right} and orientation matrix R_{right} which are defined in the calibration range coordinate system. Taking the left camera as the reference system, the relative relation of these two cameras can be represented as

$$\begin{cases} R_{l/r} = R_{left}^{-1} \cdot R_{right} \\ T_{l/r} = R_{left}^{-1} \cdot (T_{right} - T_{left}) \end{cases} \quad (3)$$

where $R_{l/r}$ and $T_{l/r}$ are the right camera's orientation and translation relative to the left camera.

To validate the effectiveness of our model of calibration, we performed many outdoor experiments. By comparing our measurements with ground check points measured by differential GPS, the three dimensional measurement accuracy is consistent with the theoretical accuracy. The height accuracy is within 0.5 m using the calibrated parameters, meeting the accuracy requirement for near-region terrain correction.

2.4 Calibration of the rotary stage

The acquisition of panoramic images around the survey station is realized by rotating the rotary stage. Thus, the exterior orientation parameters of the images are determined by the rotary stage's horizontal (azimuth) and vertical (tilt) angles. Ideally, after the rotary stage is leveled, the cameras move on a horizontal plane when the rotary stage rotates horizontally, and move on two vertical planes when the rotary stage rotates vertically. In reality, due to the installation limitations and errors, there are unavoidable offsets for the rotating axes and the rotating centers. In order to get accurate exterior orientation parameters, the actual position and orientation of both vertical and horizontal rotating axes should be determined.

We establish the rotary stage coordinate system as Fig.5

illustrates: the origin is set to be the center of the baseline of the stereo cameras; the X and Z axis lie on the horizontal base plane and the Y axis lies vertically; L_v is the vertical rotating axis and L_H is the horizontal rotating axis. In order to calibrate these two rotating axes' offsets and the origin offset, the rotary stage is set to be within the three dimensional calibration range. A series of images are taken at different horizontal and vertical angles: first, the rotary stage rotates -35° vertically and then rotates -360° horizontally at 5° intervals and stereo images are acquired at these stops; second, the rotary stage rotates vertically by an increment of 5° and the process of horizontal rotation and image acquisition repeats as in the first step; the vertical rotation finishes until the vertical angle reaches 35° . Through space resection with collinearity equations, a series of camera's discrete orientation can be determined and the camera's circular trajectory can be fitted through a least squares solution. As a rotating axis is orthogonal to the corresponding circular trajectory, its actual location and orientation can be determined, which are as $A_p^H(p_1, v_1)$ and $A_p^V(p_2, v_2)$ for horizontal and vertical axis respectively. Here, p_1 and v_1 represent the position and orientation of the vertical rotation axis while p_2 and v_2 represent the position and orientation of the horizontal rotation axis.

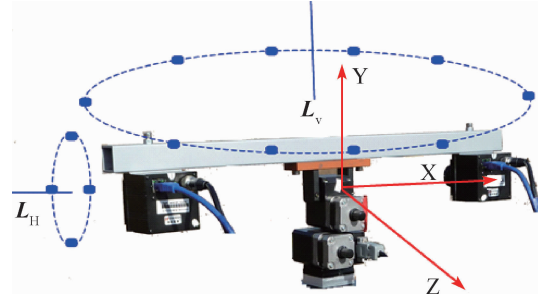


Fig.5 Rotary stage coordinate system

2.5 Calculation of exterior camera parameters

When the rotary stage's horizontal and vertical angles are set to 0, the initial state of stereo cameras in the rotary stage coordinate system can be calculated as

$$\begin{cases} R_{l0} = R(v_2) \cdot R(v_1) \cdot R(0,0,0) \\ T_{l0} = R_{l0} \cdot ((-L/2, 0, 0)^T - p_1) \\ R_{r0} = R(v_2) \cdot R(v_1) \cdot R(v_{r1}) \cdot R(0,0,0) \\ T_{r0} = R_{r0} \cdot ((L/2, 0, 0)^T - p_2) \end{cases} \quad (4)$$

where L is the baseline length of stereo cameras, R_{l0} and T_{l0} denote the left camera's initial exterior parameters (rotation matrix and translation vector), R_{r0} and T_{r0} denote the right camera's initial exterior parameters.

Given the rotary stage's horizontal angle θ and vertical angle ϕ , the camera's exterior parameters R and T can be accurately calculated as

$$\begin{cases} R = R(\phi, 0, 0) \cdot R(0, \theta, 0) \cdot R_0 \\ T = R \cdot T_0 \end{cases} \quad (5)$$

where R_0 and T_0 are camera's initial state and are substituted by R_{l0} , T_{l0} and R_{r0} , T_{r0} to calculate the left and right camera's exterior orientation parameters.

3 THREE-DIMENSIONAL TERRAIN RECONSTRUCTION AND NEAR REGION TERRAIN CORRECTION

The software system can generate near region terrain correction value automatically by the means of batch processing based on panoramic stereo images captured around the survey station, which largely reduces manual labor. There are mainly two steps in the process: (1) three-dimensional point cloud generation and filtering in order to produce high quality DEM; (2) topographic correction based on the DEM. The flowchart of this process is illustrated in Fig.6.

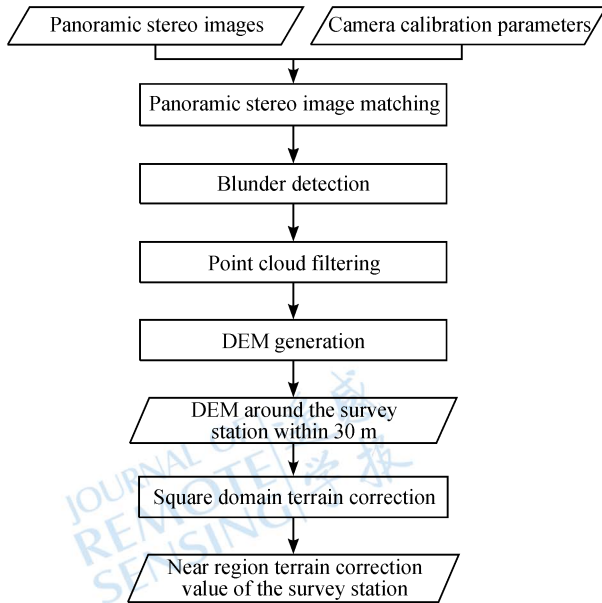


Fig.6 Flowchart of three-dimensional terrain reconstruction and gravity terrain correction

3.1 Point cloud generation and blunder detection

First, radiometric enhancement is conducted by Gaussian filter to remove image noises. Then, by applying Förstner operator (Förstner & Güelch, 1987) with proper threshold, mass feature points are detected in the images. To make the detected points well distributed in the whole image and adaptive to local terrain conditions, the image is divided into tens of grids and in each grid certain amount of points are detected by adjusting the operator threshold within the grid. Afterwards, stereo image matching is performed by using normalized correlation coefficients method on the detected feature points from the stereo images. Least squares matching method is further applied to achieve sub-pixel matching precision. Constraints of local disparity consistency and epipolar geometry are imposed to improve the reliability and efficiency of the stereo matching. Finally, three-dimensional positions of the matched points are calculated using space intersection with collinearity equations. Generally, more than 6000 three-dimensional points are generated this way at one station using 12 pairs of stereo images.

It is usually unavoidable that blunder exists in three

dimensional point cloud. A blunder detection algorithm (Li & Zhu, 2000) is adopted. The main idea of the algorithm is as the following: (1) for each point P , a window with fixed size centered at P is defined and the median height value is found within the window; (2) if the difference between the height and the median is above a certain threshold, P is detected as a blunder and removed. The above threshold is determined automatically by a statistical analysis: (1) for each window, the difference of each point's height with the mean height value of the rest of the points within the window is calculated; (2) the threshold is three times of the root mean square difference.

3.2 Point cloud filtering and terrain reconstruction

As above-earth points are also mixed in the point cloud, they need to be removed in order to reconstruct bare-earth terrain. A slope-based morphological filtering algorithm (Vosselman, 2000) is applied for this purpose. Point cloud is filtered by defining such a slope-based core function represented as:

$$\left\{ \begin{array}{l} \Omega = \{ p_i \in A \mid \forall p_j \in A : |h_{p_i} - h_{p_j}| \leq \Delta h_{\max}(d(p_i, p_j)) \} \quad (6) \\ \Delta h_{\max} = \theta_{\text{slope}} \times d \end{array} \right.$$

where d is the horizontal distance between the two points, θ_{slope} is the slope threshold, Δh_{\max} is the maximum height difference, Ω is the filtered point cloud. A point is accepted only when the height difference between the point and other points in the neighborhood is not above Δh_{\max} . By traversing the point cloud, all the above-earth points are rejected.

However, it is difficult to define a uniform slope threshold as the terrain varies. An adaptive point cloud filtering algorithm (Zhou, 2004) is applied to tackle the problem. The algorithm mainly includes the following steps: (1) by dividing the point cloud using sparse grid, an adaptive slope threshold for each grid is determined through plane fitting using the three dimensional points within the sparse grid cell; (2) for each sparse grid, filter out the points which don't obey the rule described by Eq.(6); (3) by dividing the point cloud using dense grid, a similar procedure of (1) and (2) is applied; (4) by reducing the sparse grid width by a factor of 2, the iteration continues until the sparse grid width equals the dense grid width. In our experiment, the widths of the sparse and dense grids are set to be 5 m, 0.5 m respectively.

As the three dimensional points are defined in the rotary stage's coordinated system (leveled through the tripod), in order to obtain the three dimensional points' absolute height in geodetic coordinate system, the gravity station's absolute height and the rotary stage's relative height above the earth are needed. For each survey station, the absolute geodetic height can be obtained by GPS while the relative height is manually measured by a steel tape. It is worth to note that absolute azimuthal correction is not needed for the purpose of topographic correction.

Finally, DEM can be reconstructed from filtered three dimensional point clouds by kriging interpolation method.

3.3 Topographic correction

As the automatically generated DEM is stored as square grid data, topographic correction value is conveniently calculated

with square domain method (Jiang, 1988; Shen, 1993; Feng, 2007). Fig.7 shows how this terrain correction method is performed around the survey station.

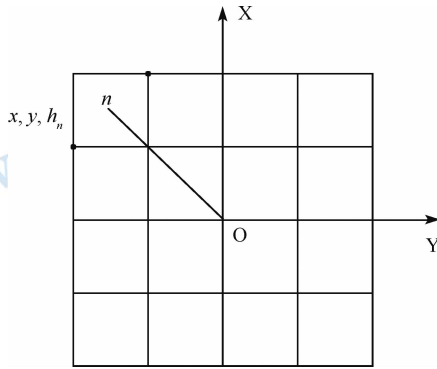


Fig.7 Square domain method for topographic correction

In Fig.7, O is the survey station and n is the center of the grid cell with the grid size of 1 m (such a resolution meets the requirement of near-region terrain gravity correction). Then the terrain correction value of that grid is calculated as (Jiang, 1988)

$$\Delta g_n = f\sigma \iint \left(1 - \frac{\sqrt{x^2 + y^2}}{\sqrt{x^2 + y^2 + h_n^2}} \right) \frac{1}{(x^2 + y^2)^{1/2}} dx dy \quad (7)$$

where $f=6.67 \times 10^{-8}$ is the gravitational constant, σ is density of rocks constructing the terrain, x and y are the horizontal and vertical coordinate in the survey station coordinate system, h_n is the

grid cell's absolute height.

By summing up all grid cells' terrain effects, the gravity correction value of the survey station is finally calculated as

$$\Delta g = \sum \Delta g_n \quad (8)$$

4 EXPERIMENTAL RESULTS

Experiments and field tests have been performed to verify the developed system. In the field test in the area of Ming Tombs in Beijing suburb, panoramic stereo images were collected at 15 stations with various terrain circumstances. Here we report the results of two typical gravity stations. The terrain of station A is relatively flat; station B has larger terrain relief and slopes. Panoramic images at the two stations are shown in Fig.8 and Fig.9 respectively. DEMs of the two stations (60 m×60 m) are automatically generated with a required 1 m resolution. Fig.10 shows the DEM of station A before and after point cloud filtering. Fig.11 shows the DEM of station B before and after point cloud filtering. Here X,Y and Z are horizontal and vertical coordinate in the survey station coordinate system. As we can clearly see from Fig.8, the environment surrounding the gravity station is covered with a lot of grass, which poses a real challenge for image matching and DEM generation. As a result, many blunders appear randomly in the generated DEM without point cloud filtering. From the final DEMs, it can be seen that point cloud filtering can effectively remove blunders and above-earth points.

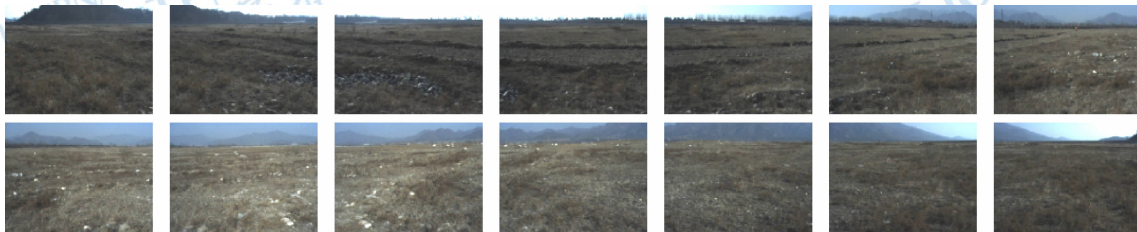


Fig.8 Panoramic image sequences of station A

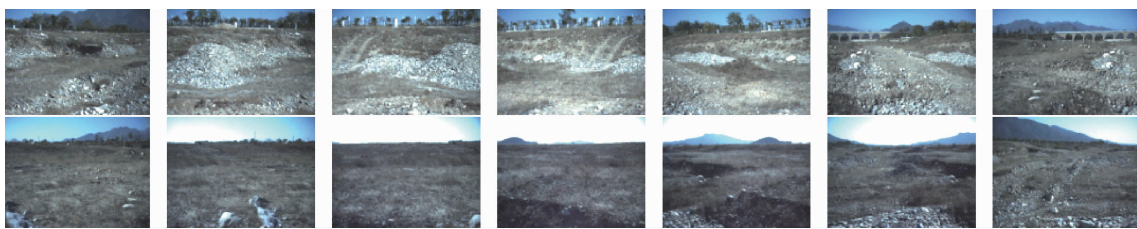


Fig.9 Panoramic image sequences of station B

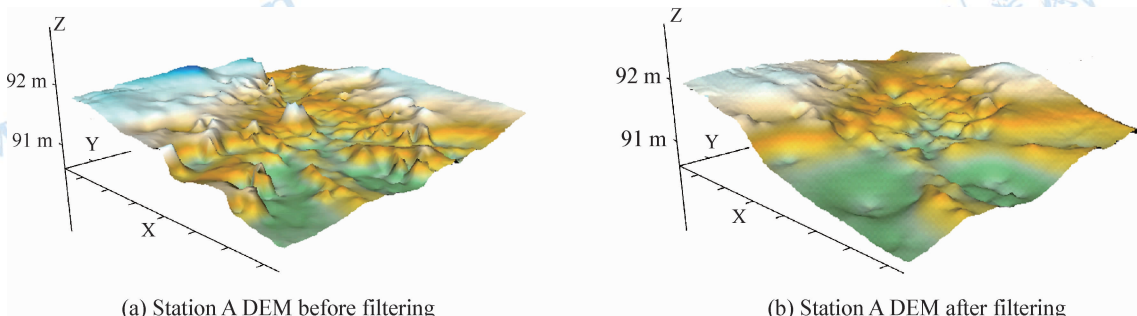


Fig.10 Station A DEM

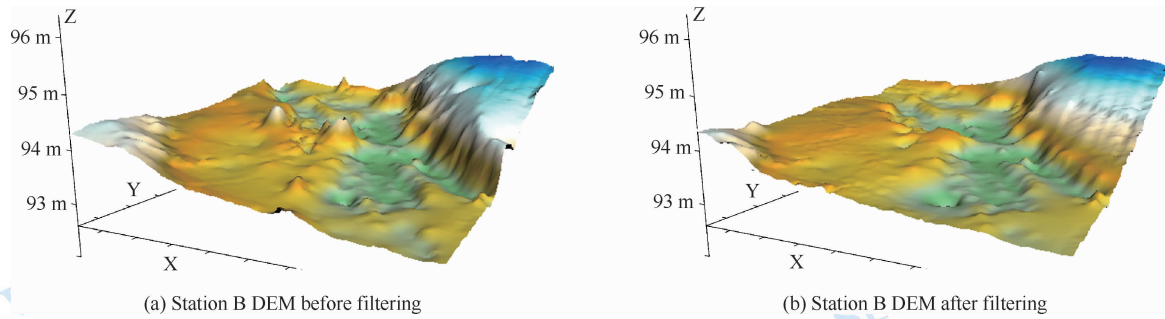


Fig.11 Station B DEM

In order to evaluate the accuracy of terrain reconstruction and correction, 1:500 large-scale maps and high quality DEMs of the field test area were produced through a large-scale filed survey using differential GPS and total station with high density of sampling points, at least one point per square meter. The densely measured ground points, DEM and derived topographic correction values are used as ground truths (references) in the following comparisons.

In our experiments, we evaluate the DEM accuracy using a series of check points (60 points for A and 89 points for B) evenly distributed in the 60 m×60 m square areas by comparing the heights at given horizontal positions with their actual height values. Fig.12 and Fig.13 are the height error histograms of the two DEMs. The RMSEs are 0.46 m and 0.84 m respectively, which satisfy the required accuracy of 1 m.

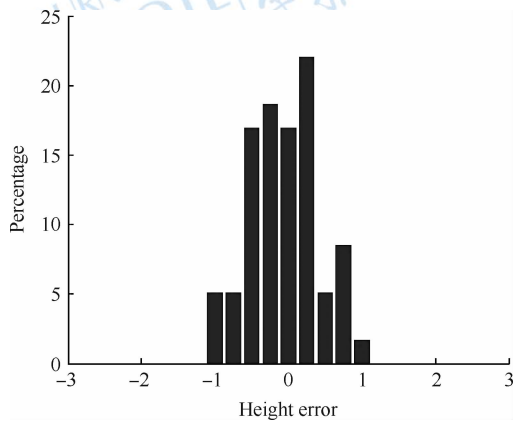


Fig.12 Station A DEM error histogram

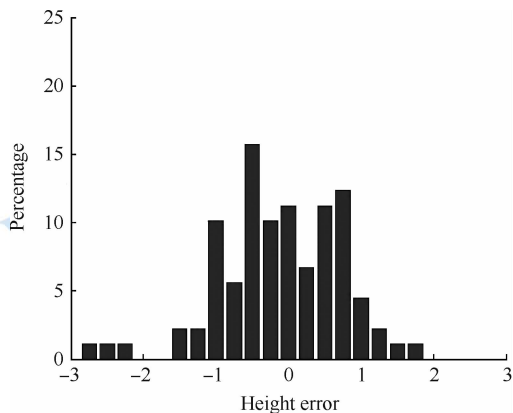


Fig.13 Station B DEM error histogram

It can be seen from the figures that the error distributions generally satisfy normal distribution. Meanwhile, the height accuracy of the flatter terrain is better than that of the terrain with larger slopes. This is due to two reasons: occlusions are likely to exist in the images of the terrain with larger slopes which may decrease the final accuracy; horizontal accuracy has a larger effect on height accuracy of the DEM in larger slopes. Overall, the actual mapping accuracy is generally consistent with the theoretical accuracy.

Having obtained the DEM for each station, the topographic correction values from our new method are calculated and compared with the reference values and the values calculated from the traditional method of total-station based field surveying. The reference topographic correction values are derived from high qualities DEMs mentioned above (derived from very dense ground points measured by differential GPS and total station), while the correction values of the traditional method are calculated from sparse ground points (40 points in each gravity station) measured by total station. Table 2 shows the comparison results.

Table 2 Topographic correction accuracy comparison

Station No.	Reference/mgal	Traditional method/mgal	New method/mgal	Error for traditional method/mgal	Error for new method/mgal
1	0.04353	0.05775	0.04541	0.01422	0.00188
2	0.01705	0.03091	0.0157	0.01386	-0.00135
3	0.00958	0.00005	0.01200	-0.00953	0.00242
4	0.00612	0.00277	0.0087	-0.00335	0.00258
RMSE/mgal				0.01114	0.00211

From Table 2 above, the accuracy of our new method is much higher than that of the traditional field surveying method. In fact, the RMSE gets largely decreased from 0.01114 mgal to 0.00211 mgal by using our new method compared to the traditional methods. Since our mapping system automatically collects much denser three-dimensional points of the terrain than traditional field surveying, thus the overall accuracy of the DEM for topographic correction is generally higher. This is particularly significant for mountainous areas where the traditional method would need to measure more points in order to achieve satisfactory accuracy.

Referring to efficiency, for each station the panoramic image (12 stereo pairs) acquisition time is about 60 s and the

automatic DEM generation time is about 35 s. For most of the test stations, the terrain correction process is fully automatic without human intervention. For some stations where there are dense trees, some manual operation is necessary, which may take several minutes. Overall, in addition to accuracy improvement, this is a significant improvement in efficiency over the traditional field surveying method.

5 CONCLUSIONS

In this paper, we presented a fast near-region gravity terrain correction approach based on panoramic vision. As a complete system, the hardware design, system calibration, theoretical accuracy, and the automated DEM generation techniques are described. The experimental results demonstrate that the developed system significantly outperforms the traditional field surveying method in efficiency and accuracy. The aim of the system is to reach the required accuracy with low-cost and reliable hardware components along with dedicated software, rather than to achieve highest accuracy using high-end hardware components. The software system will be further enhanced in the future. More field tests will be performed to validate this new system so that it can be applied in practical applications in topographic correction for regional gravity survey.

REFERENCES

- Bott M H P. 1959. The use of electronic digital computers for the evaluation of gravimetric terrain corrections. *Geophysical Prospecting*, 7(1): 45-54 [DOI: 10.1111/j.1365-2478.1959.tb01452.x]
- Campbell D L. 1980. Gravity terrain corrections for stations on a uniform slope—a power law approximation. *Geophysics*, 45(1): 109-112 [DOI: 10.1190/1.1441035]
- Cogbill (Allen) H. 1990. Gravity terrain corrections calculated using digital elevation models. *Geophysics*, 55(1): 102-106 [DOI: 10.1190/1.1442762]
- Di K C and Ge Z J. 2011. A brief review of Spirit's six years of Mars roving and scientific discoveries. *Journal of Remote Sensing*, 15(4): 651-658
- Di K C and Li R X. 2007. Topographic mapping capability analysis of mars exploration rover 2003 mission imagery // *Proceedings of 5th International Symposium on Mobile Mapping Technology (MMT 2007)*. Padua, Italy: 28-31
- Di K C and Peng M. 2011. Wide baseline mapping for mars rovers. *Photogrammetric Engineering and Remote Sensing*, 77(6): 609-618
- Di K C, Wu K, Liu Z Q, Wan W H, Di Z Z and Li G. 2011. A fast topographic mapping system based on panoramic vision for near region terrain correction in region gravity survey // *Proceedings of the 32nd Asian Conference on Remote Sensing*. Taipei, China
- Fan X F. 2007. On fast calculation for the near region terrain correction of the regional gravity survey. *Chinese Journal of Engineering Geophysics*, 4(6): 560-562
- Feng W H. 2002. Close-range camera calibration // Wang J L, ed. *Close-range Photogrammetry*. Wuhan: Wuhan University Press: 185-215
- Feng Z H. 2007. A tentative discussion on the median region gravity terrain correction method in regional gravity survey. *Geophysical and Geochemical Exploration*, 31(5): 455-459
- Förstner W and Güelch E. 1987. A Fast operator for detection and precise location of distinct points, corners and centers of circular features // *ISPRS Intercommission Workshop on Fast Processing of Photogrammetric Data*. Interlaken, Switzerland: 281-305
- Hammer S. 1939. Terrain corrections for gravimeter stations. *Geophysics*, 4(3): 184-194 [DOI: 10.1190/1.1440495]
- Heikkila J and Silven O. 1997. A four-step camera calibration procedure with implicit image correction // *Proceedings of the IEEE Computer Society Conference on Computer Vision and Pattern Recognition*. San Juan, Puerto Rico: IEEE, 1106-1112 [DOI: 10.1109/CVPR.1997.609468]
- Jia R Z, Davis L and Groom R W. 2009. New approaches to topographic gravity corrections // *Proceedings of the 22th EEGS Symposium on the Application of Geophysics to Engineering and Environmental Problems*. Texas: Curran Associates
- Jiang Y L. 1988. Research on near region gravity correction method of square domain. *Geology and Exploration*, 5: 37-40
- Kane M F. 1962. A comprehensive system of terrain corrections using a digital computer. *Geophysics*, 27(4): 455-462 [DOI: 10.1190/1.1439044]
- Klingele E. 1980. A new method for near-topographic correction in gravity surveys. *Pure and Applied Geophysics*, 119(2): 373-379 [DOI: 10.1007/BF00877772]
- Leanman D E. 1998. The gravity terrain correction-practical considerations. *Exploration Geophysics*, 29(4): 467-471 [DOI: 10.1071/EG998467]
- Li Z H, Li Q and Lin X. 2011. Research on the terrain correction models in gravity survey. *Engineering of Surveying and Mapping*, 20(2): 24-26
- Li Z L and Zhu Q. 2000. *Digital Terrain Model*. Wuhan: Wuhan Technical University of Surveying and Mapping Press: 93-101
- Nagy D. 1966. The prism method for terrain corrections using digital computers. *Pure and Applied Geophysics*, 63(1): 31-39 [DOI: 10.1007/BF00875156]
- Parker R L. 1996. Improved Fourier terrain correction, Part II. *Geophysics*, 61(2): 365-372 [DOI: 10.1190/1.1443965]
- Shen Z M. 1993. Programming of near-region terrain correction for high precision gravity survey. *Computing Techniques for Geographical and Geochemical Exploration*, 15(2): 175-177
- Sun W K and Ding P F. 1997. DZ/T 0171-1997 Large scale gravity exploration specification. Ministry of Geology and Mineral Resources. pp. 5-6
- Vosselman G. 2000. Slope based filtering of laser altimetry data. *International Archives of Photogrammetry and Remote Sensing*, Amsterdam, XXXIII: 935-942
- Yang Y B, Han G M and Liang M. 2011. Gravity near zone terrain correction precision discussion. *Computing Techniques for Geophysical and Geochemical Exploration*, 33(1): 92-96
- Yen H Y, Yeh Y H and Chen C H. 1994. Gravity terrain corrections of Taiwan. *Terrestrial, Atmospheric and Oceanic Sciences*, 5(1): 1-10
- Zhang Z X and Zhang J Q. 1997. *Digital Photogrammetry*. Wuhan: Wuhan Technical University of Surveying and Mapping: 171-172
- Zhou F C. 2004. *An Adaptive Point Cloud Filtering Algorithm for DEM Generation from Airborne Lidar Data*. Taiwan: Cheng Kung University: 27-42
- Zhou X, Zhong B and Li X. 1990. Gravimetric terrain corrections by triangular-element method. *Geophysics*, 55(2): 232-238 [DOI: 10.1190/1.1442831]

全景立体视觉的快速近区重力地形改正方法

邸凯昌¹, 吴凯¹, 刘召芹¹, 万文辉¹, 邸志众², 李钢²

1. 遥感科学国家重点实验室, 中国科学院遥感与数字地球研究所, 北京 100101;

2. 北京勘察技术工程有限公司, 北京 100085

摘要:重力地形改正是区域重力测量工作中的一个关键步骤,按照测区范围分为近区、中区和远区地形改正。中区和远区的地形改正基于已有的中小比例尺地形数据库比较容易实现,但近区地形改正对于地形产品精度的要求较高而相应的大比例尺地形数据缺乏,实际作业中仍然需要外业大量的人工采点和内业处理生成近区地形,严重制约了重力测量工作的精度和效率。因此,如何快速价廉地重建重力测站附近高精度的3维地形,成为目前高精度区域重力测量工作中亟待解决的具有挑战性的问题。

本文提出了一种基于全景立体视觉和摄影测量技术的快速近区重力地形改正方法,设计和开发了相应的快速地形测图系统,能够自动生成近区高精度的数字地形模型并解算出相应的近区重力地形改正值,从而实现了近区地形改正的高精度和自动化。系统的设计思想是在满足精度要求的前提下集成价廉可靠的硬件单元并开发专门软件实现可应用推广的系统,而不是采用昂贵的高端硬件以达到最高的精度。

全景立体测图系统的硬件单元包括两台工业相机与固定基线构成的立体相机、双自由度(水平 $\pm 180^\circ$, 竖直 $\pm 36^\circ$)旋转云台和支撑采集设备的三脚架,并通过笔记本控制云台和立体相机采集测站周围的影像。这些硬件的选取与配置基于理论精度分析与设计优化,结果表明测站50 m范围内的3维测量精度优于1 m,满足近区地形改正的精度需求。为了实现理论上的测图精度,采用控制点均匀分布的3维控制场,对立体测图系统的几何参数进行了精确标定,其中包括相机的内参数、畸变系数、立体相机的相对位置姿态以及云台旋转轴和中心的偏移参数。

基于标定后测图系统精准的几何参数,从360°全景立体影像建立无缝的立体模型,采用兴趣点提取、自相关和最小二乘匹配等技术实现快速立体影像匹配,进而通过空间前方交会计算生成测站30 m范围内的均匀密集点云;再通过点云滤波自适应去除粗差点,采用Kringing插值算法自动生成数字高程模型DEM,从而快速重建测站附近高精度的3维地形;最后利用方域公式计算得到测点周边精确的近区地形改正值。经过野外多站多种地形的实验验证,基于本文所提出的方法及所开发的地形改正系统在5 min内即可完成外业采集和内业生成地形改正值的一体化处理,效率和精度明显优于传统的野外测量方法。

关键词:重力地形改正,地形测图,全景视觉,立体影像匹配,点云滤波

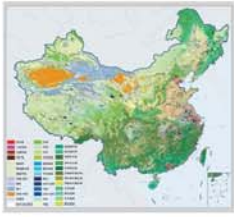
中图分类号: TP79 **文献标志码:** A

引用格式: 邸凯昌, 吴凯, 刘召芹, 万文辉, 邸志众, 李钢. 2013. 全景立体视觉的快速近区重力地形改正方法. 遥感学报, 17(4): 759-767

Di K C, Wu K, Liu Z Q, Wan W H, Di Z Z and Li G. 2013. Fast near-region gravity terrain correction approach based on panoramic stereo vision. *Journal of Remote Sensing*, 17(4): 759-767 [DOI: 10.11834/jrs.20132218]

收稿日期: 2012-07-17; 修订日期: 2012-12-26; 优先数字出版日期: 2013-01-03

基金项目: 国家重点基础研究发展计划(973计划)(编号: 2012CB719902); 国家自然科学基金(编号: 41171355); 北京勘察技术工程有限公司的资金
第一作者简介: 邸凯昌(1967—), 男, 教授, 主要研究方向为行星遥感制图与探测车导航定位。E-mail: kcidi@irsa.ac.cn



封面说明

About the Cover

2010年中国土地覆被遥感监测数据集 (ChinaCover2010)

The China National Land Cover Data for 2010 (ChinaCover2010)

2010年中国土地覆被遥感监测数据集 (ChinaCover2010) 由中国科学院遥感与数字地球研究所联合其他9个单位历时两年完成, 应用30 m空间分辨率的环境星 (HJ-1A/1B) 数据, 利用联合国粮农组织 (FAO) 的LCCS分类工具, 构建了适用于中国生态特征的38类土地覆被分类系统, 采用基于超算平台的数据预处理、面向对象的自动分类、地面调查获得的10万个野外样本以及雷达数据辅助分类相结合的方法, 数据精度达到85%。ChinaCover2010主要基于国产卫星影像, 将遥感与生态紧密结合, 充足的野外样点以及严格的产品质量控制在最大程度上保证了数据的精度, 可为中国生态环境变化评估以及生态系统碳估算提供基础数据支撑。(网址: <http://www.chinacover.org.cn>)

The China National Land Cover Data for 2010 (ChinaCover2010) has been completed after two years of team effort by the Institute of Remote Sensing and Digital Earth (RAD), Chinese Academy of Sciences (CAS), together with nine other institutions' participation. The HJ-1A/1B satellite at 30 m resolution is main data source. Based on the landscape features in China, 38 land cover classes have been defined using UN FAO Land Cover Classification System (LCCS). Super computers were used in the data preprocessing. An object-oriented method and a thorough field survey (about 100000 field samples) were used in the land cover classification, with radar imagery as auxiliary data. The overall accuracy of ChinaCover2010 is around 85%. Mainly based on domestic imagery, the products take advantage of various in situ data and strict quality control. ChinaCover2010 is a good dataset for ecological environment change assessment and terrestrial carbon budget studies. (Website: <http://www.chinacover.org.cn>)

遥感学报

JOURNAL OF REMOTE SENSING

YAOGAN XUEBAO (双月刊 1997年创刊)

第17卷 第4期 2013年7月25日

(Bimonthly, Started in 1997)

Vol.17 No.4 July 25, 2013

主 管	中国科学院	Superintended	by	Chinese Academy of Sciences
主 办	中国科学院遥感与数字地球研究所 中国地理学会环境遥感分会	Sponsored	by	Institute of Remote Sensing and Digital Earth, CAS The Associate on Environment Remote Sensing of China
主 编	顾行发	Editor-in-Chief		GU Xing-fa
编 辑	《遥感学报》编委会 北京市安外大屯路中国科学院遥感与数字地球研究所 邮编: 100101 电话: 86-10-64806643 http://www.jors.cn E-mail: jrs@irsa.ac.cn	Edited	by	Editorial Board of Journal of Remote Sensing Add: P.O.Box 9718, Beijing 100101, China Tel: 86-10-64806643 http://www.jors.cn E-mail: jrs@irsa.ac.cn
出 版	科学出版社	Published	by	Science Press
印刷装订	北京科信印刷有限公司	Printed	by	Beijing Kexin Printing Co. Ltd.
总 发 行	科学出版社 北京东黄城根北街16号 邮政编码: 100717 电话: 86-10-64017032 E-mail: sales_journal@mail.sciencep.com	Distributed	by	Science Press Add: 16 Donghuangchenggen North Street, Beijing 100717, China Tel: 86-10-64017032 E-mail: sales_journal@mail.sciencep.com
国外发行	中国国际图书贸易总公司 北京 399 信箱 邮政编码: 100044	Overseas distributed	by	China International Book Trading Corporation Add: P.O.Box 399, Beijing 100044, China

中国标准连续出版物号: ISSN 1007-4619

国内邮发代号: 82-324

定价: 70.00元

ISSN 1007-4619

CODEN YXAUAB

CN 11-3841/TP

国外发行代号: BM 1002

国内外公开发行

